Acta Astronautica 103 (2014) 36–44

Contents lists available at ScienceDirect

Acta Astronautica

journal homepage: www.elsevier.com/locate/actaastro

A bionic approach to mathematical modeling the fold geometry of deployable reflector antennas on satellites

C.M. Feng, T.S. Liu *,[1]

Department of Mechanical Engineering, National Chiao Tung University, Hsinchu 30010, Taiwan

ARTICLE INFO

Article history:
Received 7 January 2014
Received in revised form
19 June 2014
Accepted 20 June 2014
Available online 28 June 2014

Keywords:
Deployable reflector antenna
Deployable membrane reflector
Bionics design
Fold geometry
Morphological change

ABSTRACT

Inspired from biology, this study presents a method for designing the fold geometry of deployable reflectors. Since the space available inside rockets for transporting satellites with reflector antennas is typically cylindrical in shape, and its cross-sectional area is considerably smaller than the reflector antenna after deployment, the cross-sectional area of the folded reflector must be smaller than the available rocket interior space. Membrane reflectors in aerospace are a type of lightweight structure that can be packaged compactly. To design membrane reflectors from the perspective of deployment processes, bionic applications from morphological changes of plants are investigated. Creating biologically inspired reflectors, this paper deals with fold geometry of reflectors, which imitate flower buds. This study uses mathematical formulation to describe geometric profiles of flower buds. Based on the formulation, new designs for deployable membrane reflectors derived from bionics are proposed. Adjusting parameters in the formulation of these designs leads to decreases in reflector area before deployment.

1. Introduction

Construction in a low- or no-gravity environment is difficult. Thus, deployable devices are widely used in space technologies due to their low construction expenses, light weights, and high packing efficiencies [1]. Solar panels, reflectors, radars, and satellite masts are examples of such deployable devices and are generally constructed to be deployable so that they are compact during launch [2–6]. Large reflectors with 4 to 25 m diameter are considered for future satellites dedicated to earth observation, telecommunication and science missions [7]. A rigid reflector of this diameter range will not fit in most launch vehicles for transportation into orbit. Table 1 lists fairing diameters of Delta series launch vehicles [8]. To lower the launch volume and weight of the device, the reflector can be constructed to be deployable, as has been suggested from observations of several radar missions [9–11]. Because the space inside a rocket is cylindrical in shape and has a cross-sectional area that is much smaller than the satellite antenna after deployment, the question of how to decrease the cross-sectional area of the folded reflector is an important task.

Most deployable reflectors can be divided into two types: solid surface reflectors [12–14] and membrane surface reflectors [15–17]. Membrane reflectors are compactly stowed before deployment and can be expanded to obtain large reflective area. Most materials used in the construction of membrane reflectors are polymers onto which thin metal films are coated to reflect electromagnetic waves. These metal layers may generate gaps or cracks due to the large curvatures experienced when the

* Corresponding author. Tel.: +886 3 5712121x55123; fax: +886 3 5720634.
E-mail address: tsliu@mail.nctu.edu.tw (T.S. Liu).
[1] Postal address: EE405, 1001 University Road, Hsinchu 30010, Taiwan, ROC.

http://dx.doi.org/10.1016/j.actaastro.2014.06.029
0094-5765/

Table 1
Fairing diameter of Delta series launch vehicles [8].

Type	Diameter (m)
Delta II 2.9-m	2.540
Delta II 3-m	2.743
Delta II 3-m stretched	2.743
Delta III 4-m	3.749
Delta IV M	3.750
Delta IV M+	4.572
Delta IV heavy	4.572
Delta IV heavy aluminum isogrid	4.572
Delta IV heavy dual manifest	4.572

reflector is folded before deployment. These gaps and cracks will effect the electromagnetic wave patterns of reflector antennas [18].

To design deployable membrane reflectors, this study learns from the biological world. Nature has elegantly crafted efficient solutions to many of the same or similar problems as those faced by engineers [19]. Solutions have evolved in several biological systems including insect wings, plant leaves, and flower petals [20,21]. To design deployable antennas for use in satellite, this paper aims to develop a bionic approach to designing geometric profiles of membrane reflectors that look like the bud of a morning glory, a twining or vine-like plant when folded. This study formulates geometric profiles for folded membrane reflectors that are derived from bionics. These are then used as the basis for new designs of deployable membrane reflectors.

2. Fold geometry design

Nature supplies a rich variety of design references for the creation of products. Morphological changes in nature provide a source of design inspiration. This paper deals with the fold geometry of reflectors by observing morphological changes of flower blooms. Fig. 1(a) and (b) respectively show blooming morning glory and bindweed [20]. Bindweed belongs to the morning-glory family [22,23]. Accordingly, both flowers have similar geometric profiles before and after bloom. From the viewpoint of geometric profiles, this study treats both flowers to be the same. Initially, petals of each flower constitute a funnel-form corolla. The petals in turn gradually expand to full bloom. In bloom processes of both flowers transforming from closed buds to the blossomy shape, the petals do not split into several lobes. In the top view of both flower buds, the petal profile consists of several concavities and bulges in cyclic arrangement. During blooming, the profile maintains axial symmetry and gradually becomes circular. The variation of profiles in the top view can be drawn as geometric curves, as shown in Fig. 1(c). This study constructs mathematical models to describe the geometric profile of morning glory buds. Although, several deployable reflector designs [24,25] in the literature are similar to the bloom process of the morning glory, such as an example shown in Fig. 2, mathematical models were not created.

2.1. Geometric profile formulation

The geometries of many membrane reflectors resemble the morning glory in full bloom. A deployed reflector can be folded in a manner similar to the folding of a morning glory bud. To facilitate the folding of the reflector, the geometric profile of the reflector cross-section is designed as a ring. Fig. 3(a) and (b) depict a reflector before deployment (i.e., after folding), treated as a morning glory bud in this study, and after deployment, respectively.

The cross-sectional profile of a folded reflector, as depicted in Fig. 3(a), will be designed in this study with reference to the morning glory bud. The outermost profile curve of the reflector cross-section before deployment is depicted in Fig. 4 and can be formulated in polar coordinates r and θ

$$r_c(\theta) = A\ \cos\left(B\ \sin\left(\frac{n\theta}{2}\right)\right) \tag{1}$$

where A is the maximum radius of the cross-sectional profile, B is defined as the concavity factor of the curve, and n denotes the number of petals of the bud. As B increases, notches between two adjacent petals will deepen and approach the curve center; i.e., B determines the depth of the notches between two adjacent petals, as shown in Fig. 4 at $\theta=(\pi/5)$, $(3\pi/5)$, π, $(7\pi/5)$, and $(9\pi/5)$. The curve in Fig. 4 has five identical petals, $n=5$, and a maximum radius A at $\theta=(2\pi/5)$, $(4\pi/5)$, $(6\pi/5)$, $(8\pi/5)$, and 2π. Every two neighboring radial lines intersect at the angle $(\pi/5)$. These intersecting lines thus divide the curve into 10 equal parts as shown in Fig. 4.

Using the same values of A and n as in Eq. (1), different B values will induce different concave shapes of the curve, as depicted in Fig. 5. If B equals zero, there will be no notch, and the curve obtained from Eq. (1) will be a circle with radius A. In contrast, when B equals $\pi/2$, the notches between two adjacent petals of the curve based on Eq. (1) will be so deep that the notches will intersect at the center of the curve. Although B can be any real value, to produce geometric profiles of reflectors before deployment that resemble a morning glory and to avoid the intersection of profiles at the curve center, this study confines the range of B values to between 0.6 and 1.5. As B increases, notches between two adjacent petals deepen and approach the center of the curve.

Fig. 6 depicts morning glory profiles with (a) 5, (b) 15, and (c) 25 petals, with $A=50$ and $B=0.8$. Because the same A and B values are used in Fig. 6(a) to (c), the profile curves exhibit the same radii and notch depths between two adjacent petals.

2.2. Determining the maximum radius A

If a smooth curve C is represented by $x=f(\theta)$ and $y=g(\theta)$ such that C does not intersect itself in the interval $\alpha\le\theta\le\beta$, the arc length of C over the interval is expressed by

$$s_c = \int_\alpha^\beta \sqrt{\left(\frac{dx}{d\theta}\right)^2+\left(\frac{dy}{d\theta}\right)^2}\,d\theta \tag{2}$$

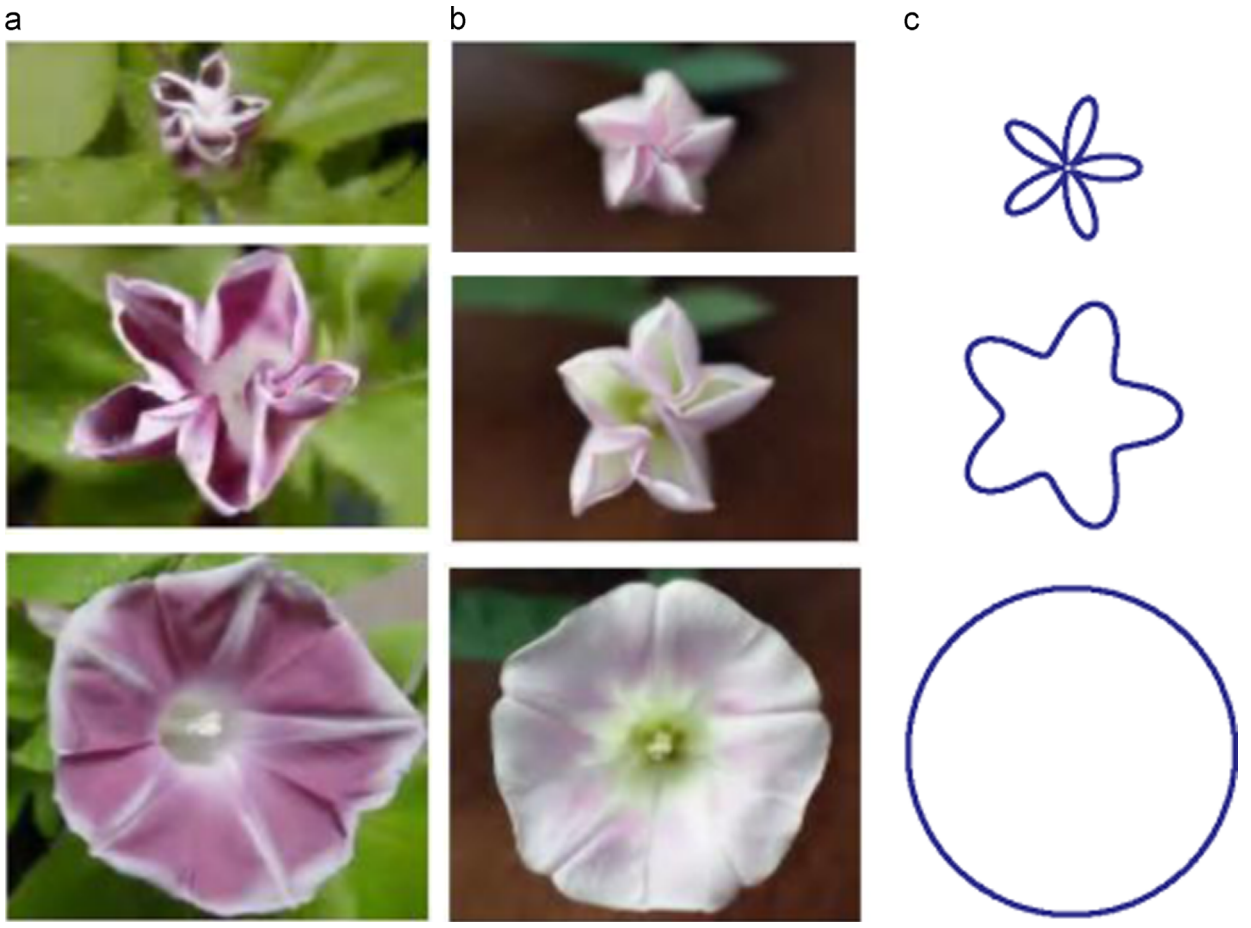

Fig. 1. Bloom processes of (a) morning glory and (b) bindweed [20]. (c) Drawings of the geometric profile based on bloom processes of both flowers in the top view.

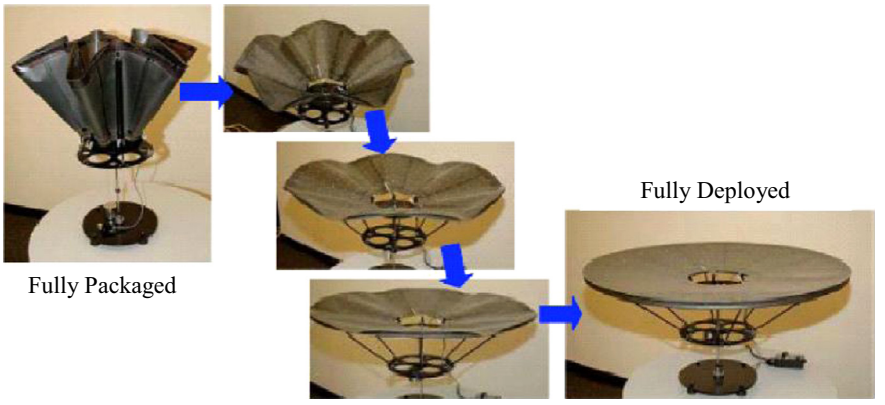

Fig. 2. Deployable reflector made of shape memory polymer [24,25].

The profile curve $r_c(\theta)$ on the cross-section of the folded reflector is represented by the following parametric equations

$$x = r_c(\theta)\cos\ \theta$$

$$y = r_c(\theta)\sin\ \theta \tag{3}$$

and

$$\frac{dx}{d\theta} = r_c'(\theta)\cos\ \theta - r_c(\theta)\sin\ \theta$$

$$\frac{dy}{d\theta} = r_c'(\theta)\sin\ \theta + r_c(\theta)\cos\ \theta \tag{4}$$

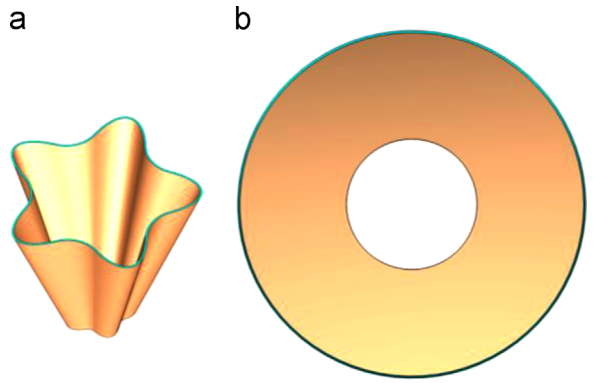

Fig. 3. Contrast between a membrane reflector with five petals (a) before and (b) after deployment.

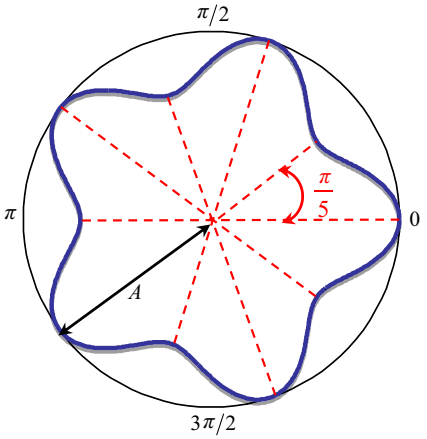

Fig. 4. Geometric curve, drawn based on Eq. (1), of the morning glory bud's petals. The radial lines divide the geometric curve into 10 equal parts, and two neighboring radial lines intersect at an angle of $\pi/5$.

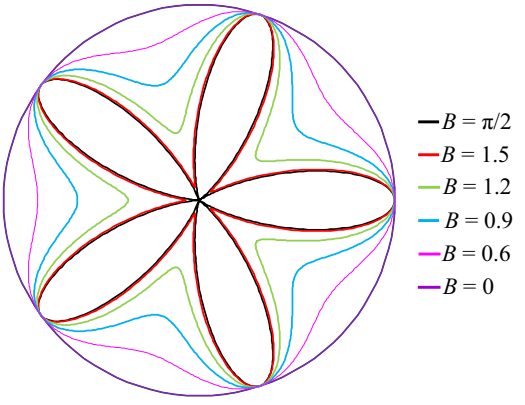

Fig. 5. Comparison among curves generated from Eq. (1). A larger concavity factor B results in deeper notches between two neighboring petals.

Eq. (4) leads to

$$\left(\frac{dx}{d\theta}\right)^2+\left(\frac{dy}{d\theta}\right)^2=[r_c'(\theta)\cos\theta-r_c(\theta)\sin\theta]^2+[r_c'(\theta)\sin\theta+r_c(\theta)\cos\theta]^2$$

$$=[r_c(\theta)]^2+[r_c'(\theta)]^2 \tag{5}$$

Using Eqs. (2) and (5), the arc length s_r of the profile curve r_c in $0\le\theta\le2\pi$ is written as

$$s_r=\int_0^{2\pi}P(\theta)d\theta \tag{6}$$

where

$$P(\theta)=\sqrt{[r_c(\theta)]^2+[r_c'(\theta)]^2} \tag{7}$$

Because the explicit integral of Eq. (6) is not available, reducing the range of θ to $0\le\theta\le\pi/n$ is necessary, and using Taylor's theorem to expand Eq. (7) about c leads to

$$P_q(\theta)=P(c)+\sum_{q=1}^{q}\frac{P^{(q)}(c)}{q!}(\theta-c)^q \tag{8}$$

In Fig. 7, function curves are drawn based on Eqs. (7) and (8). Eq. (8) is expanded about $c=\pi/(2n)$ as 5th-, 7th-, and 9th-order Taylor series. The range of θ is from 0 to π/n. The 9th-order series is close to the function $P(\theta)$. Therefore, Eq. (8) can be rewritten as the 9th-order Taylor series

$$P_9(\theta)=[0.125A^2B^2n^2\sin^2(0.707B)+A^2\cos^2(0.707B)]^{1/2}+\sum_{q=1}^{9}\frac{P^{(q)}(\pi/2n)}{q!}\left(\theta-\frac{\pi}{2n}\right)^q \tag{9}$$

$P_9(\theta)$, instead of $P(\theta)$, is substituted into Eq. (6) to calculate the arc length of the profile curve r_c of a cross-section at the top of the folded reflector shown in Fig. 3(a). Since D denotes the diameter of the reflector after deployment, the arc length of the profile curve r_c has to equal the circumference πD of the deployed reflector, shown in Fig. 3(b). Thus, $s_r=\pi D$. As θ ranges from 0 to π/n, the arc length of this interval equals $s/2n$. Therefore, Eq. (6) can be rewritten as

$$\frac{s_r}{n}=\int_0^{\pi/n}P_9(\theta)d\theta=\frac{\pi D}{n} \tag{10}$$

Solving Eq. (10) results in the maximum radius A. For example, assume that the diameter of a reflector after deployment is D, and the reflector is folded as five petals, $n=5$. The value of the concavity factor B is prescribed as 1.2. As a result, Eqs. (9) and (10) yields a maximum radius of $A=0.4D$. According to Eqs. (9) and (10), after parameters B and n have been prescribed, the value of A depends on the parameters B and n. Fig. 8 presents the maximum radius A vs. the concavity factor B with respect to different values of n. The maximum fold radius A decreases with increases in the concavity factor B or petal numbers n. Thus, it is advantageous to reduce the cross-sectional area before antenna deployment by increasing B or n.

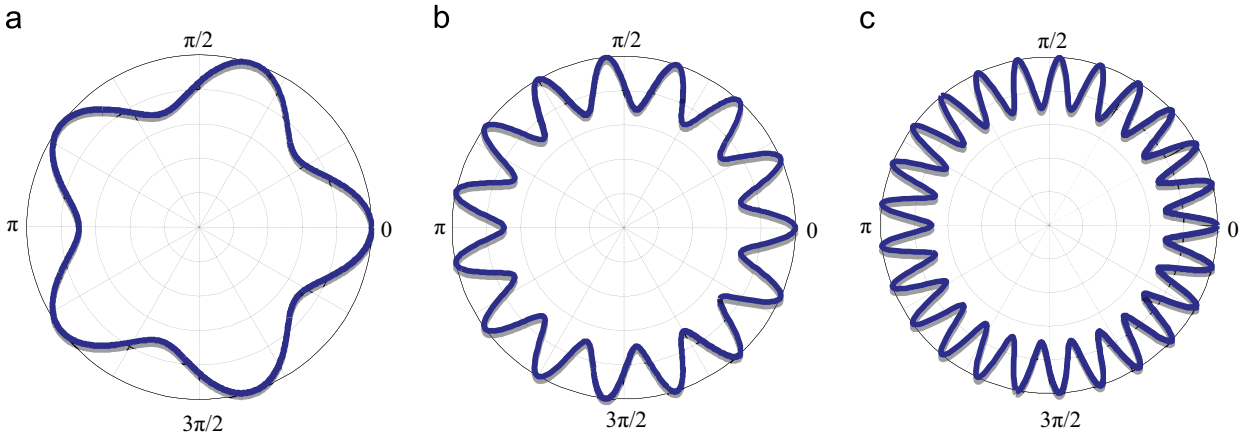

Fig. 6. Morning glory profiles of petal numbers (a) $n=5$, (b) $n=15$, and (c) $n=25$ petals, with $A=50$ and $B=0.8$.

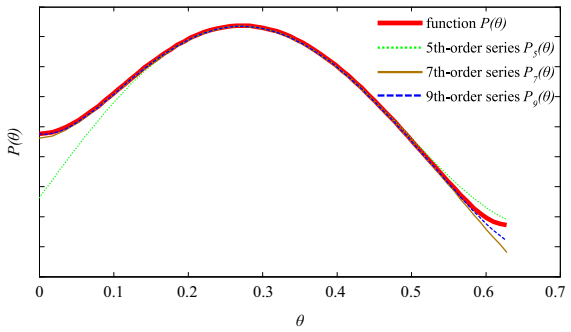

Fig. 7. Function curves drawn based on Eqs. (7) and (8). Eq. (8) is expanded about $c=\pi/10$.

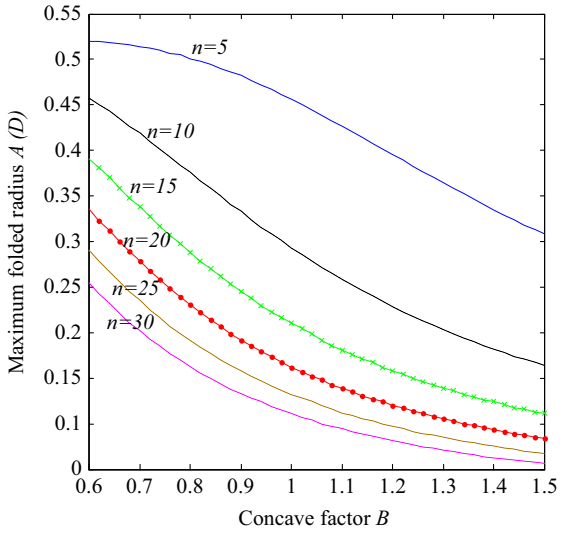

Fig. 8. Maximum radius A vs. the concavity factor B with respect to different numbers of folded petal n.

3. Curvature and cross-sectional area ratio of profile curve

It follows from Figs. 5 and 6 that the curvature of the profile curve $r_c(\theta)$ vary with the concavity factor B and the numbers of petal n, respectively. When either B or n increases beyond a certain value, the curvature at $\theta=(\pi/n)$ becomes excessive. Excessive curvature may induce the formation of a crease on the reflector surface and generate gaps or cracks in the layer of metal on the reflector. These gaps and cracks will affect the pattern of electromagnetic waves on the reflector antennas [18]. Therefore, excessive curvature should be avoided.

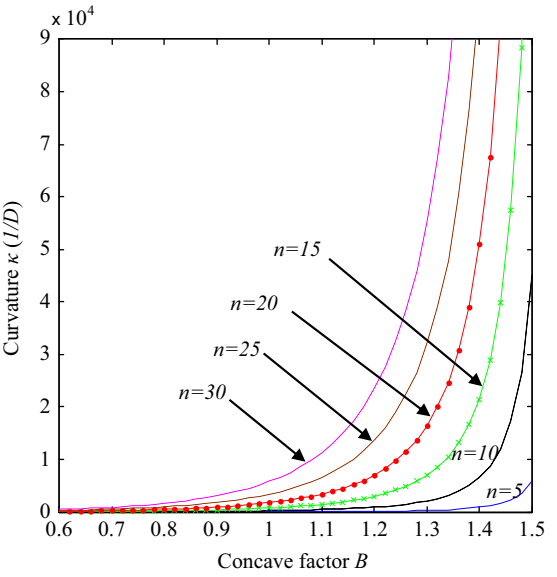

Fig. 9. Curvature κ vs. the concavity factor B with different numbers of petal n.

3.1. Determining the curvature of a curve $r_c(\theta)$

The curvature of any profile curve r_c in polar coordinates is expressed by [26]

$$\kappa(\theta)=\frac{|r_c^2+2r_c'^2-r_c r''_c|}{(r_c^2+r_c'^2)^{3/2}} \tag{11}$$

where

$$r_c' = -\frac{1}{2}ABn\ \sin\left(B\ \sin\left(\frac{n\theta}{2}\right)\right)\cos\left(\frac{n\theta}{2}\right) \tag{12}$$

and

$$r''_c = \frac{1}{4}ABn^2\ \sin\left(B\ \sin\left(\frac{n\theta}{2}\right)\right)\sin\left(\frac{n\theta}{2}\right) - \frac{1}{4}AB^2n^2\ \cos\left(B\ \sin\left(\frac{n\theta}{2}\right)\right)\cos^2\left(\frac{n\theta}{2}\right) \tag{13}$$

As depicted in Figs. 3 and 4, the maximum curvature of the profile curve r_c occurs at $\theta=\pi/n$. Therefore, substituting Eqs. (1), (12) and (13) into Eq. (11) at $\theta=\pi/n$ yields

$$\kappa\left(\frac{\pi}{n}\right) = \frac{|A^2\cos^2 B - 0.25A^2Bn^2\ \cos\ B\ \sin\ B|}{(A^2\cos^2 B)^{3/2}} \tag{14}$$

According to Eqs. (10) and (14), the curvature κ depends on parameters B and n, whose relationship is depicted in Fig. 9, where D denotes the reflector diameter after deployment.

As depicted in Fig. 9, increasing the number of folded petals n or concavity factor B will increase the curvature κ. The curvature will increase sharply when the value of B increases beyond a certain value. For example, when n and B equal 10 and 1.5, respectively, the curvature will increase sharply. With an increasing number of petals n, the critical value of B will decrease.

3.2. Cross-section areas before and after folding

This study presents mathematical models with respect to profile curves of reflector cross sections. Hence, the smaller the enclosed area of a profile curve is, the smaller the cross-section area of the reflector is. The area enclosed by a profile curve r_c can be written as [27]

$$A_f = \frac{1}{2}\int_0^{2\pi} r_c^2(\theta)d\theta \tag{15}$$

Define the integrand in Eq. (15) as

$$R = r_c^2(\theta) = A^2\cos^2\left(B\ \sin\left(\frac{n\theta}{2}\right)\right) \tag{16}$$

Because the explicit integral of R is not available, reducing the range of θ to $0\le\theta\le\pi/n$ and using the 9th-order Taylor series for the expansion of R about $c=\pi/(2n)$ leads to

$$R_9(\theta) = A^2\cos^2(0.707B) + \sum_{q=1}^{9}\frac{R^{(q)}(\pi/2n)}{q!}\left(\theta-\frac{\pi}{2n}\right)^q \tag{17}$$

where $R_9(\theta)$ is the 9th-order Taylor series for R in Eq. (16). Therefore, Eq. (15) can be rewritten as

$$A_f = n\int_0^{\pi/n} R_9(\theta)d\theta \tag{18}$$

The outermost geometric profile of a reflector cross-section after deployment is a circle whose area is denoted as A_d. The ratio of the deployed reflector area vs. the area enclosed by the profile curve r_c is denoted as A_d/A_f, where

$$A_d = \frac{1}{2}\int_0^{2\pi} R_d^2(\cos^2\theta + \sin^2\theta)d\theta \tag{19}$$

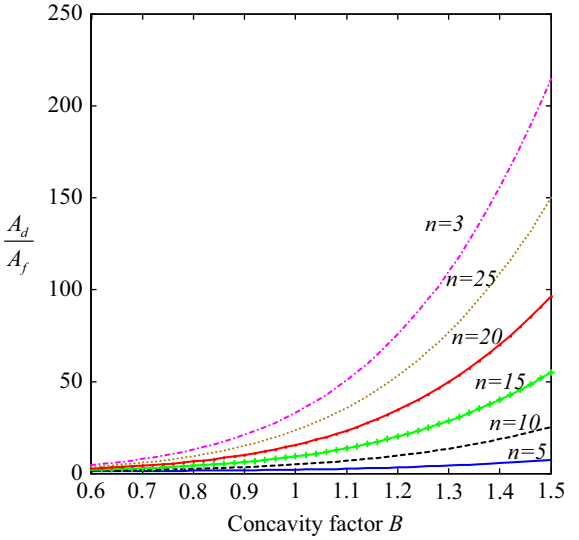

Fig. 10. Ratios of the deployed reflector areas to the areas enclosed by the profile curve r_c.

Table 2
Geometric profile designs with different values of B and n.

Design	Concavity factor B	Number of petals n	Curvature at θ/n (1/cm)	Fold diameter (cm)
a	0.9	5	0.04	491
b	1.4	5	1.72	342
c	1.2	10	1.81	233
d	1	15	1.49	214
e	0.9	20	1.84	196
f	0.8	25	1.88	195
g	0.7	30	1.67	206
h	1.2	30	46.44	83

Larger ratios represent larger gains in antenna area after deployment relative to the same antenna before deployment. Obtaining a larger gain in area is the present design goal. Fig. 10 presents A_d/A_f ratios vs. the concavity factor B with different numbers of folded petals n. Increasing the concavity factor B or petal numbers n will effectively reduce the pre-deployment reflector area. However, as shown in Fig. 9, the curvature of the profile curve r_c will increase sharply when B and n increase beyond a certain value. Increasing B and n results in smaller pre-deployment cross-sectional areas, but also larger curvatures.

4. Discussion

Concerning reflector diameter examples, Rao et al. [28] have presented an antenna, used in L-band communication, with a parabolic reflector of diameter 510 cm. However, the

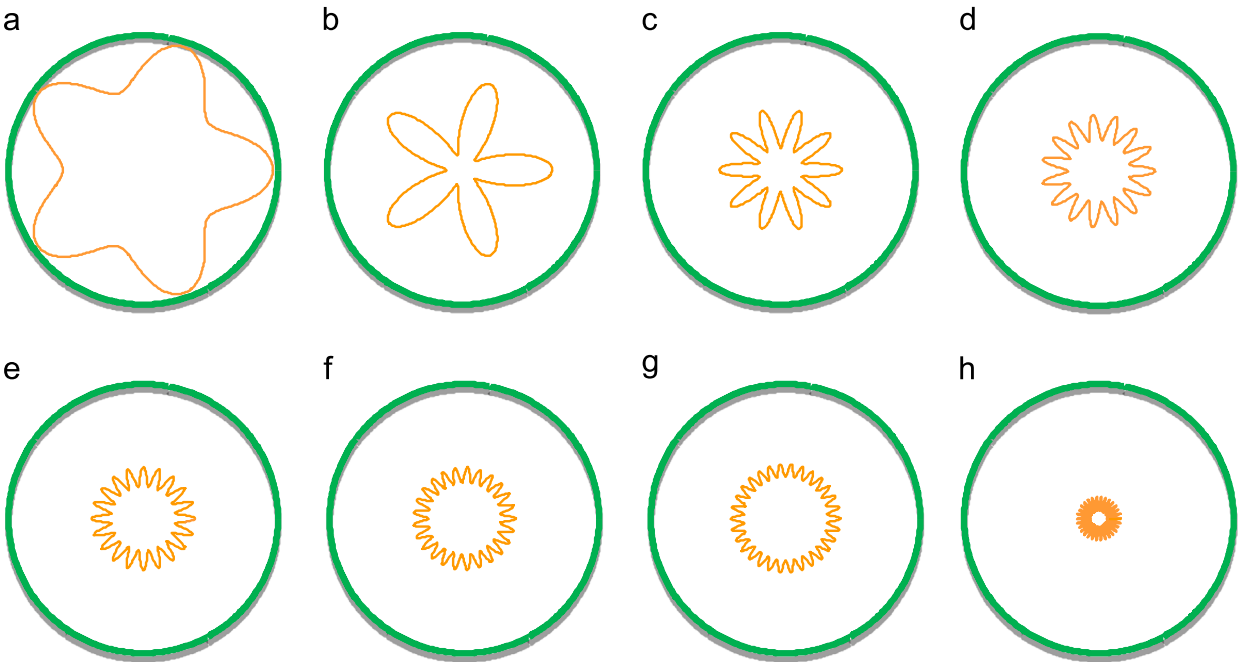

Fig. 11. Comparison of cross-sectional profiles before and after deployment: (a) $B=0.9$; $n=5$, (b) $B=1.4$; $n=5$, (c) $B=1.2$; $n=10$, (d) $B=1$; $n=15$, (e) $B=0.9$; $n=20$, (f) $B=0.8$; $n=25$, (g) $B=0.7$; $n=30$, and (h) $B=1.2$; $n=30$ based on Eqs. (1) and (10). Parameters B and n in Eq. (1) are from Table 1, and parameter A is obtained by solving Eq. (10). The outermost circles represent the cross-sectional profiles of the deployed reflectors and all have the same 510 cm radius. The star-like curves inside each graph represent the cross-sectional profiles of the folded reflectors.

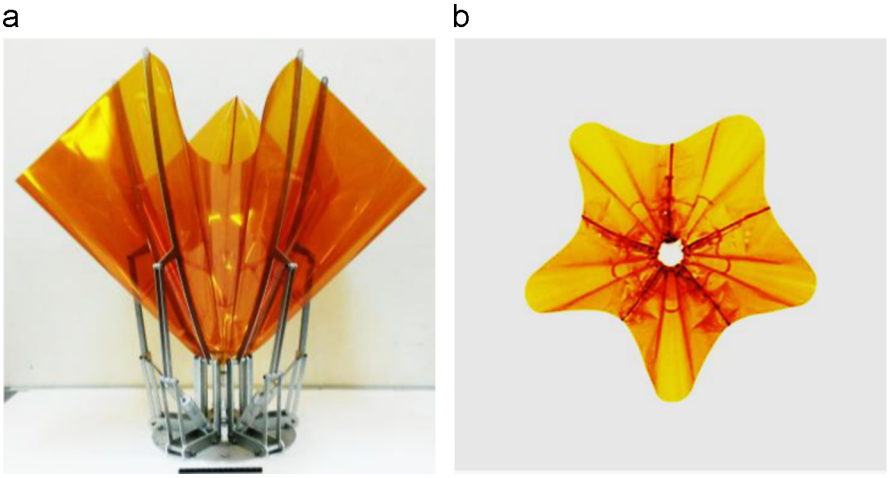

Fig. 12. Photos of the fold geometry using the proposed method in (a) front view and (b) top view of the reflector.

diameter of unfolded reflectors is too large to be placed inside the launch vehicles whose fairing diameters are listed in Table 1. Using the proposed method, as shown in Table 2 this study designs eight geometries with different values of B and n. The curvatures of designs (b) to (g) are close, ranging from 1.49 to 1.88 (1/cm). In contrast to the other designs, designs (a) and (h) have excessively small and large curvatures, respectively, and are thus inadequate designs.

Fig. 11 compares the areas of the deployed reflector and the reflector designs listed in Table 2, which are calculated based on Eqs. (1) and (10). Fig. 11(a) and (b) have the same number of petals, $n=5$, with different concavity factors B. As B increases, the enclosed areas of the profile curves decrease. Comparing Fig. 11(b) and (c), the curvatures at θ/n of the profile curves are similar. However, the enclosed area in (c) is much smaller than that in (b). Accordingly, to obtain an effective fold, the profile curve r_c should possess more than 10 petals. Therefore, (a) and (b) are ineffective designs. The designs in Fig. 11(c) to (g) all have different numbers of petal and concavity factors. These five designs are effective at shrinking the enclosed areas of the profile curves to approximately 82–88% of the deployed area. In Fig. 11(c) and (h), the profile curves have different numbers of petals n but the same concavity factor. As n increases, the enclosed areas of the profile curves

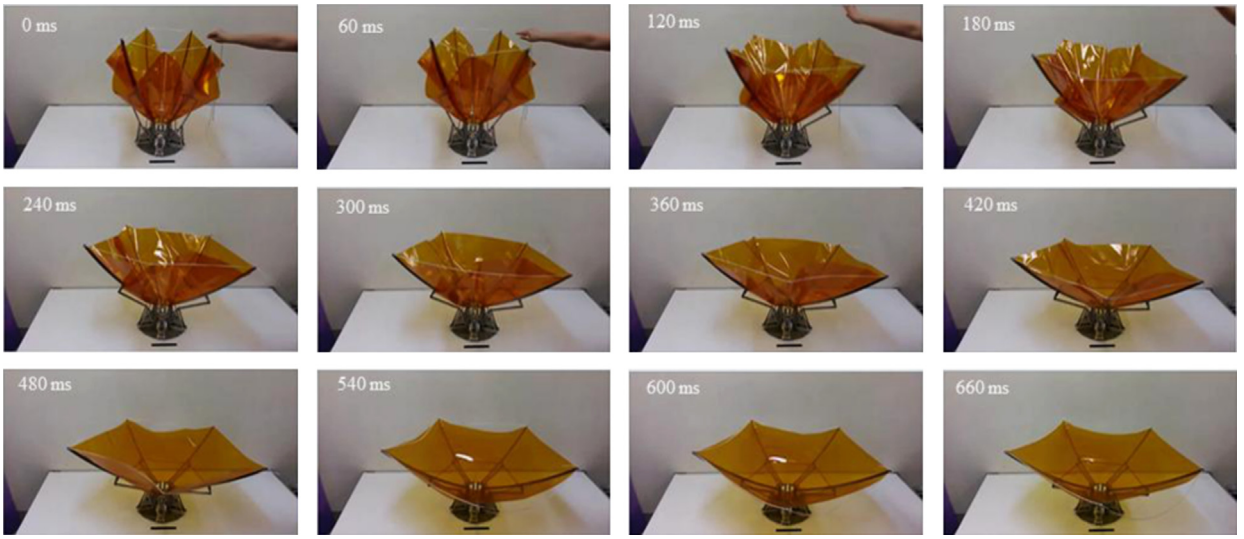

Fig. 13. Subsequent to Fig. 12, deployment process of the deployable reflector fabricated in this study.

decrease. Although design (h) reduces the area of the folded reflector by more than 95%, its excessive curvatures should be avoided. Accordingly, (h) is treated as an inadequate design. To demonstrate the proposed method for the geometric profile design of fold reflectors, as depicted in Fig. 12, this study has fabricated a membrane reflector with five petals in the fold state. Kapton membranes are pasted on parabolic ribs of a deployable mechanism [29], which can fold the membrane in a manner similar to morning glory buds with five petals. This reflector with a 120 cm diameter after deployment was folded by the deployable mechanism to produce five petals with a concavity factor of $B=0.9$. Fig. 13 shows the deployment process of this reflector.

5. Conclusion

Inspired by biological patterns, this study has investigated fold geometry for satellite deployable antennas. The profiles of folded reflectors have been formulated in polar coordinates r and θ. Adjusting parameters in the formulation leads to decrease in reflector area after fold. Fig. 11(c) to (g) illustrate that the cross-sectional area before deployment and after fold can be effectively reduced when the profile curve r_c has more than 10 petals. Dealing with the example with 510 cm unfold diameter in Discussion, this study proposes five geometric profile designs used to fold membrane reflectors, as depicted in Fig. 11(c) to (g) that are applicable to and contribute to the design of deployable antennas.

Acknowledgments

The authors would like to thank National Space Organization in Taiwan, ROC, for financial support and helpful discussions.

References

[1] P. Gruber, S. Hauplik, B. Imhof, K. Ozdemir, R. Waclavicek, M. A. Perino, Deployable structures for a human lunar base, Acta Astronaut. 61 (2007) 484–495.
[2] R.E.McVey, S.F. Bassily, Apparatus and Method for Combined Redundant Deployment and Launch Locking of Deployable Satellite Appendages, U.S. Patent 5996940, 1999.
[3] D.S. Adams, M. Mobrem, Lenticular jointed antenna deployment anomaly and resolution onboard the Mars express spacecraft, J. Spacecraft Rockets 46 (2) (2009) 403–410.
[4] R.G. Cobb, J.T. Black, E.D. Swenson, Design and flight qualification of the rigidizable inflatable get-away-special experiment, J. Spacecraft Rockets 47 (4) (2010) 659–669.
[5] S.A. Lane, T.W. Murphey, M. Zatman, Overview of the innovative space-based radar antenna technology program, J. Spacecraft Rockets 48 (1) (2011) 135–145.
[6] H.M.Y.C. Mallikarachchi, S. Pellegrino, Quasi-static folding and deployment of ultrathin composite tape-spring hinges, J. Spacecraft Rockets 48 (1) (2011) 187–198.
[7] L. Datashvili, S. Endler, B. Wei, H. Baier, H. Langer, M. Friemel, N. Tsignadze, J. Santiago-Prowald, Study of mechanical architectures of large deployable space antenna apertures: from design to tests, CEAS Space J. 5 (2013) 169–184.
[8] BOEING, Delta Expendable Launch Vehicles, URL: ⟨http://www-eng.lbl.gov/~lafever/SNAP/OldFiles/DELTA%20PAYLOAD%20OVERVIEW.htm⟩ [cited 2 April 2014].
[9] A. Currie, M.A. Brown, Wide-swath SAR, Radar Signal Process. IEE Proc. F 139 (2) (1992) 122–135.
[10] G. Callaghan, I. Longstaff, Wide-swath space-borne SAR using a quad-element array, IEE Proc. Radar Sonar Navig. 146 (1999) 159–165.
[11] M. Suess, B. Grafmueller, R. Zahn,A novel high resolution, wide swath SAR system, in: Proceedings of the IEEE 2001 International Geoscience and Remote Sensing Symposium, 2001.
[12] I. Ohtomo, H. Kumazawa, T. Itanami, K. Ueno, A. Kondo, T. Yasaka, K. Nakajima, Y. Kawakami, M. Misawa, On-board multibeam deployable antennas using Ka, C, and S frequency bands, IEEE Trans. Aerosp. Electron. Syst. 28 (4) (1992) 990–1001.
[13] S.D. Guest, S. Pellegrino, A new concept for solid surface deployable antenna, Acta Astronaut. 38 (2) (1996) 103–113.
[14] R. Taylor, D. Turse, Large Aperture, Solid Surface Deployable Reflector, NASA NNX09AD57G (2010).
[15] M.R. Johnson, The Galileo high gain antenna deployment anomaly, in: 28th Aerospace Mechanisms Symposium, NASA Conference Publication, 1994 (CP-3260).
[16] S. Pellegrino, Deployable membrane reflectors, in: Proceedings of the Second World Engineering Congress, Sarawak, 2002, 1–9.
[17] T. Takano, K. Miura, M. Natori, E. Hanayama, T. Inoue, T. Noguchi, N. Miyahara, H. Nakaguro, Deployable antenna with 10 m maximum

diameter for space use, IEEE Trans. Antennas Propag. 52 (1) (2004) 2–11.
[18] R.A. Shore, A.D. Yaghjian, Application of incremental length diffraction coefficients to calculate the pattern effects of the rim and surface cracks of reflector antenna, IEEE Trans. Antennas Propag. 41 (1) (1993) 1–11.
[19] C.H. Jenkins, J.J. Larsen, Deployment schemes for 2-D space apertures and mapping for bio-inspired design, Proceedings of the Sixth International Conference on Computation of Shell and Spatial Structures (2008). (Ithaca, NY).
[20] N. Kishimoto, M.C. Natori, K. Higuchi, K. Ukegawa, New deployable membrane structure models inspired by morphological changes in nature, in: 47th AIAA/ASME/ASCE/AHS/ASC Structures, Structural Dynamics, and Materials Conference (2006). (Newport, Rhode Island).
[21] H. Kobayashi, K. Horikawa, Y. Morita, Unfolding of potato flower as a deployable structure, Proceedings of the Sixth International Conference on Computation of Shell and Spatial Structures (2008). (Ithaca, NY).
[22] D.D. Spaulding, Key to the Bindweeds (*Calystegia* and *Convolvulus*, *Convolvulaceae*) of Alabama and Adjacent States, Phytoneuron vol. 83 (2013) 1–12.
[23] D.F. Austin, Convolvulaceae morning glory family, J. Arizona-Nevada Acad. Sci. 30 (2) (1998) 61–83.
[24] Y. Liu, H. Du, J. Leng, Shape memory polymers and their composites in aerospace applications: a review, Smart Mater. Struct. 23 (2014) 1–22.
[25] P.N. Keller, M.S. Lake, D. Codell, R. Barrett, R. Taylor, M.R. Schultz, Development of elastic memory composite stiffeners for a flexible precision reflector, in: 47th AIAA/ASME/ASCE/AHS/ASC Structures, Structural Dynamics, and Materials Conference (2006). (Newport, Rhode Island).
[26] W.A. Granville, D. Joyner, Differential Calculus and SAGE, revised ed., Wikisource (2013). (Chapter 12, URL).
[27] R. Larson, R.P. Hostetler, B.H. Edwards, Calculus with Analytic Geometry, seventh ed. Houghton Mifflin Company, Boston, 2002.
[28] B.R. Rao, W. Kunysz, R. Fante, K. McDonald, GPS/GNSS Antennas, Artech House, 2012.
[29] C.M. Feng, T.S. Liu, A graph-theory approach to designing deployable mechanism of reflector antenna, Acta Astronaut. 87 (2013) 40–47.